European Journal of Medicinal Chemistry 213 (2021) 113163

Contents lists available at ScienceDirect

European Journal of Medicinal Chemistry

journal homepage: http://www.elsevier.com/locate/ejmech

Research paper

A theranostic probe of indoleamine 2,3-dioxygenase 1 (IDO1) for small molecule cancer immunotherapy

Ying Wu [a, 1], Yanhui Zhang [b, 1], Xi Chen [b, 1], Yulu Hu [b], Guoqiang Dong [a], Yuan Guo [b, **], Chunquan Sheng [a, *]

[a] School of Pharmacy, Second Military Medical University, 325 Guohe Road, Shanghai, 200433, China
[b] Key Laboratory of Synthetic and Natural Functional Molecule of the Ministry of Education, College of Chemistry and Materials Science, Northwest University, 1 Xuefu Avenue, Xi'an, 710127, China

ARTICLE INFO

Article history:
Received 6 October 2020
Received in revised form
30 December 2020
Accepted 4 January 2021
Available online 13 January 2021

Keywords:
IDO1
Theranostic probe
Cancer immunotherapy

ABSTRACT

Discovering novel small molecules for cancer immunotherapy represents a promising but challenging strategy in future cancer treatment. Herein, we designed the first theranostic fluorescent probes to efficiently detect and inhibit the enzymatic activity of 2,3-dioxygenase 1 (IDO1). Probe **6b** is a highly active IDO1 inhibitor (IC_{50} = 12 nM, Cellular IC_{50} = 10 nM), which can sensitively and specifically detect endogenous IDO1 in living cells. Furthermore, as a theranostic probe, **6b** showed excellent *in vivo* antitumor efficacy in the CT26 xenograft mouse model as well. Therefore, it can be applied as a valuable chemical tool for better understanding the immunotherapy mechanism of IDO1 and improving the therapeutic efficiency.

1. Introduction

In recent years, there have been remarkable advances in cancer immunotherapy [1]. Immune checkpoint antibodies targeting programmed cell death protein 1 (PD-1), programmed death ligand 1 (PD-L1) and cytotoxic T-lymphocyte associated antigen 4 (CTLA-4) have achieved great clinical success in cancer treatment with superior efficacy and specificity [2,3]. However, despite the advantages, only a limited number of cancer patients have benefited from these monoclonal antibodies' treatments and immune-related side effects are frequently observed. Moreover, checkpoint antibodies generally suffer from difficult and expensive manufacturing processes and unfavourable pharmacokinetic profiles such as long half-life, poor tissue and tumor penetration, and low oral bioavailability [4]. In contrast, small-molecule immuno-oncology agents generally have the advantages of reasonable pharmacokinetics, convenient oral administration, flexible treatment regimen and so on [5,6]. Therefore, small molecules provide an alternative way to improve clinical response and outcome of cancer immunotherapy when either used alone or in combination with antibodies.

Indoleamine 2,3-dioxygenase 1 (IDO1) is a well validated drug target for the development of small-molecule cancer immunotherapeutics [7]. IDO1 is a key enzyme involved in the tryptophan–kynurenine–aryl hydrocarbon receptor (Trp–Kyn–AhR) pathway which acts as an important mediator of immunosuppression in T cell–inflamed tumors [8]. IDO1 catalyzes the conversion of Trp to *N*-formyl-kynurenine (NFK), which is subsequently hydrolyzed to Kyn. The depletion of Trp and the accumulation of Kyn both contribute to the immune escape mechanism in the tumor microenvironment [9]. Overexpression of IDO1 leads to local degradation of Trp, which suppresses T cell proliferation and activity. The generation of Kyn is also immunosuppressive because of the activation of AhR pathway and the upregulation of the expansion of regulatory T cells [9]. Thus, inhibition of IDO1 is capable to restore host immune responses to eradicate cancer cells. Up to date, a large number of IDO1 inhibitors have been discovered for cancer immunotherapy [10,11]. Several IDO1 inhibitors (*e.g.* epacadostat, indoximod, BMS986205, navoximod, PF-06840003) have been developed to apply into different stages of clinical trials [12,13]. However, phase III clinical trial of epacadostat was terminated because the combination of epacadostat and PD-1 antibody pembrolizumab failed to exert therapeutic

* Corresponding author.
** Corresponding author.
E-mail addresses: guoyuan@nwu.edu.cn (Y. Guo), shengcq@hotmail.com, shengcq@smmu.edu.cn (C. Sheng).
[1] These authors contributed equally to this work.

https://doi.org/10.1016/j.ejmech.2021.113163
0223-5234/

advantages over pembrozilumab alone [14]. Consequently, there is an urgent need for better understanding the functions and mechanisms of IDO1 inhibition and discovery of similar new strategies.

Recently, the design of new IDO1 inhibitors remains an active research area [15–19]. The IDO1 inhibition mechanisms were further clarified by solving a series of X-ray crystal structures of IDO1 in complex with various inhibitors [20–22]. Moreover, IDO1-based multi-targeting strategies, such as combining IDO1/tryptophan 2,3-dioxygenase (TDO) dual inhibitors together [23] were developed to achieve better efficacy in cancer immunotherapy. Previously, we designed novel dual inhibitors for IDO1-DNA and IDO1-histone deacetylase (HDAC), which showed improved antitumor potency [24–26]. Inspired by these results, we propose that a theranostic probe for simultaneous imaging and inhibiting IDO1 could have the advantage of diagnosing and treating patients with IDO1 overexpressed cancer. In addition, theranostic IDO1 probes will be helpful for elucidating the molecular mechanism beneath immunotherapy and improving its efficacy. However, target-based theranostic probes for small-molecule cancer immunotherapy have rarely been reported. Herein, we designed the first theranostic fluorescent probes to efficiently detect IDO1 protein.

2. Results and discussion

2.1. Chemistry

It has been reported that the *meta*-bromophenyl, oxadiazole and hydroxyamidine groups in epacadostat are essential structural features of the IDO1 inhibitors [27]. As shown in Fig. 1A (PDB: 5WN8), the aminoethyl-sulfamide substituent of epacadostat was projected out of the active site of IDO1, which makes it suitable to introduce the fluorophore here at the mouth of the substrate-binding pocket without interfering with the catalytic activity of this enzyme. Based on synthetic feasibility, the sulfamide substituent was removed to form compound **2** as the pharmacophore of IDO1 probes. Since low polarity is a unique feature of protein interior microenvironment [20] we selected the environment-sensitive chemical group 4-nitro-7-aminophenzoxadiazole (NBD) [28] as the fluorophore because of its high quantum yield, specific selectivity, excellent cell penetration ability and low toxicity [29–32]. Various linkers were used to connect the pharmacophore with the fluorophore, affording potential light-up fluorescent probes **4**, **6a** and **6b**.

The synthesis methods of the probes were shown in Scheme 1. Compound **2a** was synthesized according to our well established protocols [24–26] which subsequently underwent nucleophilic substitution and deprotection to expose the hydroxyamide group to obtain target compound **4**. Compound **3** underwent nucleophilic substitution with different minocarboxylic acids to afford intermediates **5a** or **5b**. Target compounds **6a** or **6b** were synthetized by amide condensation between **5a** or **5b** and compound **2a**, followed by the deprotection reaction.

2.2. Molecular docking studies

Molecular docking experiment was further carried out to investigate the binding mode of probes with IDO1 (PDB code: 5WN8) [33] by the docking software Gold [34]. The results demonstrate that the binding modes of these probes are similar to that of epacadostat. The phenyl group and oxadiazole form π–π stacking interaction with Tyr126 and Phe163, respectively. The oxygen atom in the hydroxyamidine group coordinates to heme iron. Moreover, the oxadiazole and the nitro group of compound **4** (Fig. 1C) could form hydrogen bonds with the backbone of Gly236 and side chain of Arg231, respectively. Similarly, the nitro group of compound **6b** (Fig. 1C) also form two hydrogen bonds with the side chains of Asn240 and Arg231, correspondingly. However, there is no strong interaction between compound **6a** (Fig. 1C) and IDO1. These binding modes well explained why probes **4** and **6b** inhibited IDO1 better than probe **6a**.

2.3. Spectral properties and selectivity of probes

To evaluate the polarity sensitivity of the three probes, we explored their responsiveness to environmental polarity in the mixed solutions of 1,4-dioxane and water with different polarities. As displayed in Fig. 2A–C, when the 1,4-dioxane fraction (f_d, by volume %) in the mixture was increased from 0% to 80%, the fluorescence intensities were enhanced by a factor of 46 (for **4**, at 540 nm), 33 (for **6a**, at 542 nm) and 37 (for **6b**, at 540 nm), indicating that all three compounds are sensitive to environmental polarity, as expected.

Although the introduction of NBD endows **4**, **6a** and **6b** with the above sensitivities, their recognition of IDO1 in essence depends on whether the inhibitor moiety introduced in the molecular skeletons can bind to IDO1 protein or not. Therefore, we first evaluated their binding affinity to IDO1 *in vitro*. To facilitate this investigation, we successfully cloned and expressed IDO1 in *Escherichia coli* BL21 (DE3), and purified the protein by Ni-NTA and gel-filtration (refer to Supporting Information). Subsequently, the fluorescent responses of **4**, **6a** and **6b** towards various concentrations of IDO1 in the solution of PBS were examined (Fig. 3, Fig. 4A and Fig. 2D–F). When increasing the concentrations of IDO1, **4** and **6b** showed progressive enhancements in fluorescence intensity, especially **6b** which exhibited a 5-fold enhancement. Conversely, no significant changes were observed when various concentrations of IDO1 were tested with **6a**. Furthermore, the selectivity of **4**, **6a** and **6b** towards IDO1 was measured with a variety of enzyme species and biomolecules. As depicted in Fig. 5, no distinct fluorescence changes were observed for each compound in the absence of IDO1, and for **6a** even in the presence of IDO1, demonstrating that **4** and **6b** possess high selectivity towards IDO1. Afterwards, taking **6b** as our pioneering probe, we investigated the reaction kinetics of **6b** with IDO1. As shown in Fig. 4B, the fluorescence intensity at 532 nm gradually enhanced and reached a plateau within 60 min. Better still, the fluorescence intensity of the **6b** solution was linearly related to the concentration of IDO1 in the range of 0–10 μM. The detection limit of **6b** for IDO1 was calculated to be 10 nM at a signal-to-noise ratio of 3 (Fig. 4A), indicative of high-sensitivity to changes in the quantities of IDO1.

2.4. Ido1 inhibitory and antiproliferative activities of probes

At first, the IDO1 inhibitory potency of probes **4**, **6a** and **6b** was assayed against human recombinant IDO1 [35]. As shown in Fig. 1B, all the probes exhibited good inhibitory activity towards IDO1. Especially, probes **4** ($IC_{50} = 28$ nM) and **6b** ($IC_{50} = 12$ nM) were even more effective than the positive control epacadostat ($IC_{50} = 47$ nM). To validate whether the introduction of NBD fluorophore might cause cytotoxicity, *in vitro* antiproliferative activities were carried out against human cervical carcinoma Hela cell line and mice colorectal cancer CT26 cell line, which were easily stimulated by IFN-γ to release endogenous IDO1 [36,37]. Fortunately, all of the compounds showed no direct cytotoxicity towards these two cell lines ($IC_{50} > 100$ μM), suggesting that these probes had little effect on cell growth and were suitable for cellular IDO1 inhibition and imaging. Furthermore, their inhibitory activities against IDO1 at the cellular level were evaluated and the results showed that probes **4** and **6b** reacted even better than epacadostat. Specially, probes **4** (Cellular $IC_{50} = 15$ nM) and **6b** (Cellular $IC_{50} = 10$ nM) were capable

(A)

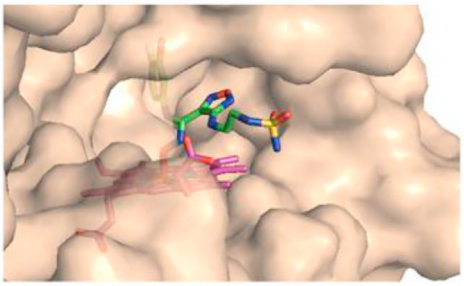

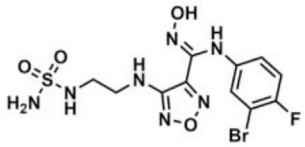

1 (epacadostat)

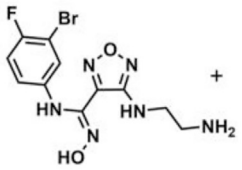

2 (epacadostat analog)

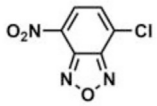

3 (NBD-Cl)

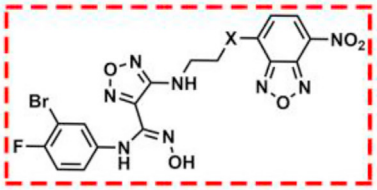

4 X = NH; 6a X = $NHCH_2CONH$;
6b X = $NHCH_2CH_2CONH$

(B)

Compounds	IDO1 (IC_{50}, nM)	CT26 (IC_{50}, μM)	Hela (IC_{50}, μM)	Hela (Cellular IC_{50}, nM)
1	47	>100	>100	19
4	28	>100	>100	15
6a	1315	>100	>100	>5000
6b	12	>100	>100	10

(C)

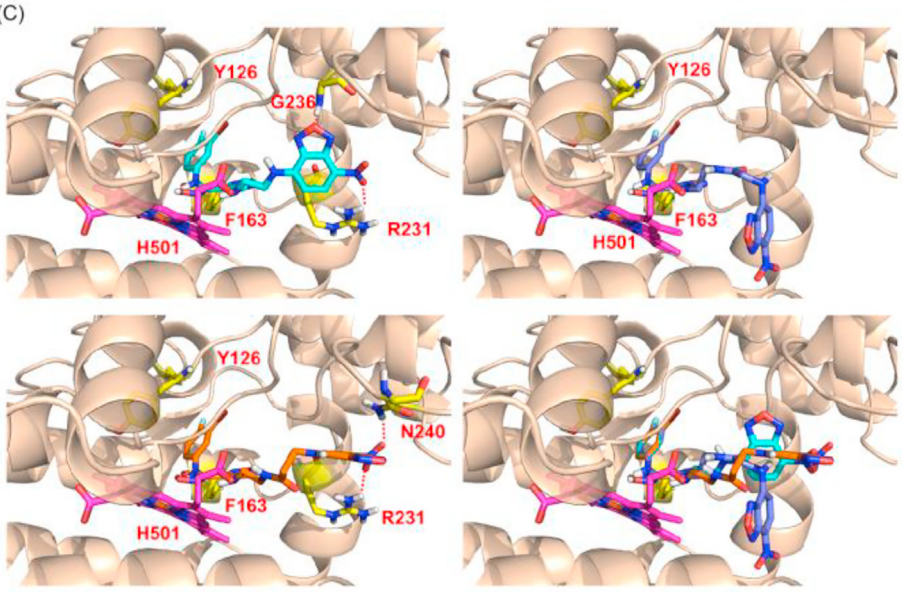

Fig. 1. Rational design, biological activity and binding mode of fluorescent probes. (A) The design rationale of IDO1 probes; (B) IDO1 enzyme inhibition and cellular potency of probes (C) Binding mode of probes **4** (cyan), **6a** (indigo) and **6b** (orange) along with their superimposition in the active site of IDO1 (PDB: 5WN8). Hydrogen bonds (red) are represented with dash lines. The figures were generated using PyMol (http://www. Pymol.org/).

of effectively transforming Trp to Kyn, whereas probe **6a** was inactive in this function.

2.5. In living cell imaging

Inspired by the favorable sensing properties of **4** and **6b** to IDO1 *in vitro*, we further investigated their application for imaging of endogenous IDO1 in living cells. As shown in Fig. 6, Hela cells stained with probe **4** or probe **6b** exhibited weak fluorescence. As expected, after stimulated by IFN-γ, Hela cells showed significant green fluorescence enhancement signals after incubation with **4** or **6b**. By contrast, Hela cells treated with IFN-γ and **6a** presented dim fluorescence signals in the green channel, which was consistent with the experimental results *in vitro*. To further verify that IDO1 is indeed responsible for the above fluorescence signals, the control imaging experiment to compete with probes for the pocket of IDO1 in living cells was carried out. When Hela cells were treated with IFN-γ and IDO1 inhibitor epacadostat, and further incubated with **4** or **6b**, fluorescence enhancement signals were not observed, which is the negative control as we anticipated. In short, these imaging

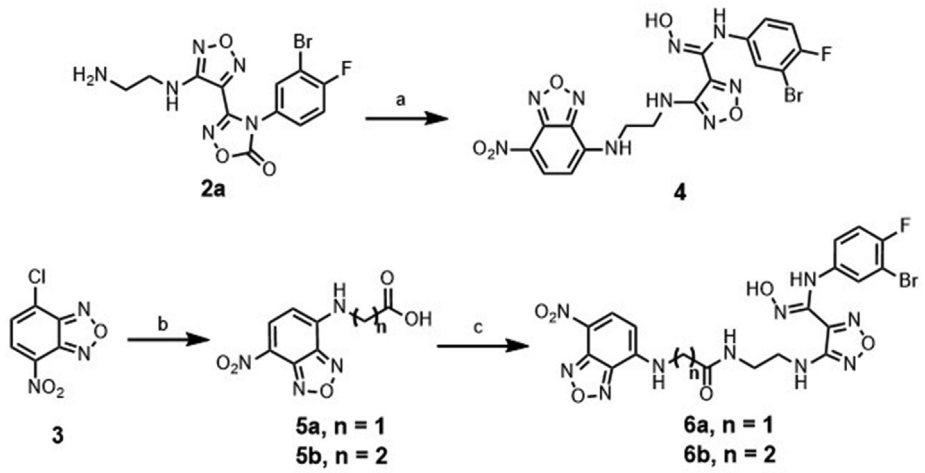

Scheme 1. Reagents and Conditions: (a) i) $NaHCO_3$, MeOH, H_2O, 60 °C, 2 h; ii) KOH, MeOH, H_2O, rt, 0.5 h, yield 28%; (b) aminocarboxylic acid, $NaHCO_3$, MeOH, H_2O, 60 °C, 2 h, yield 47–58%; (c) i) compound **2a**, HATU, DIPEA, DMF, rt, 1 h; ii) KOH, MeOH, H_2O, rt, 0.5 h, yield 14–21%.

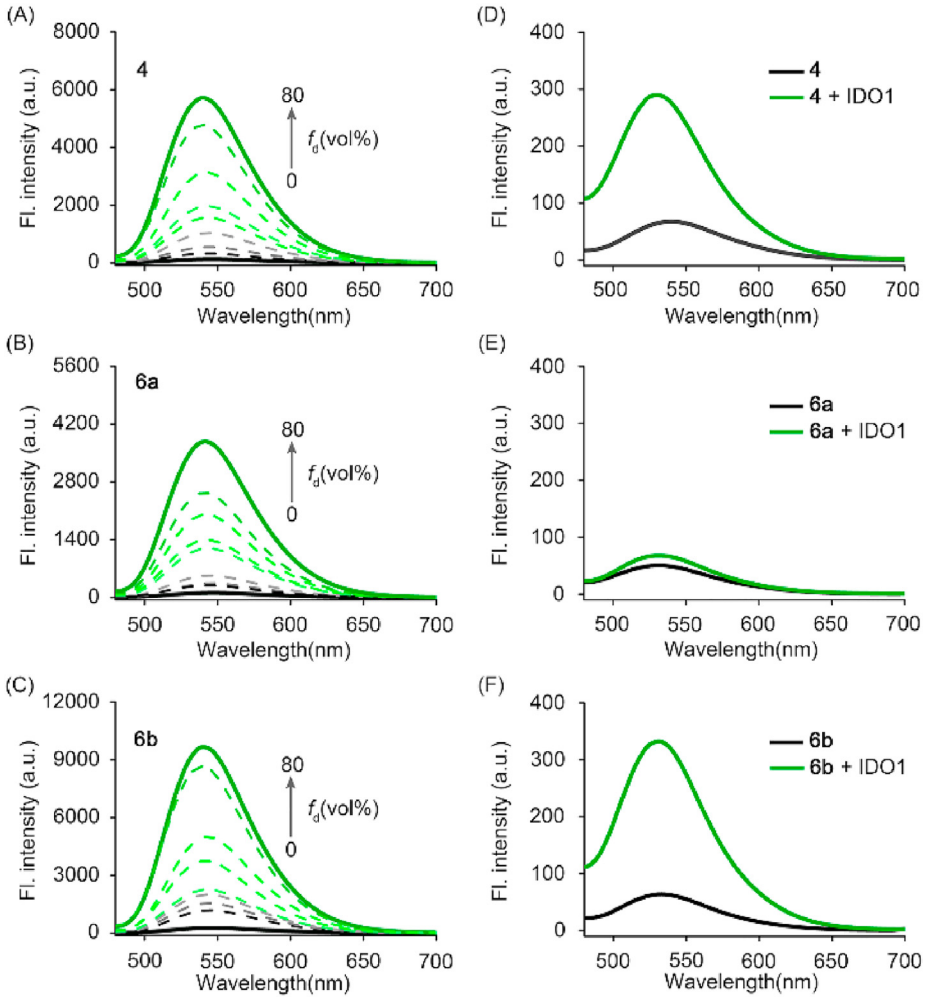

Fig. 2. Spectral properties. Fluorescence spectra of 10 μM **4** (A), 10 μM **6a** (B) and 10 μM **6b** (C) in water/1,4-dioxane mixtures with different volume fractions of 1,4-dioxane (f_d) (λ_{ex} = 465 nm, slit widths: W_{ex} = 5 nm, W_{em} = 5 nm). Fluorescence spectra of 10 μM **4** (D), 10 μM **6a** (E), and 10 μM **6b** (F) in the absence or presence IDO1 (10 μM) in PBS buffer solution (10 mM, pH = 7.4, containing 1% DMSO, λ_{ex} = 465 nm, slit widths: W_{ex} = 5 nm, W_{em} = 5 nm).

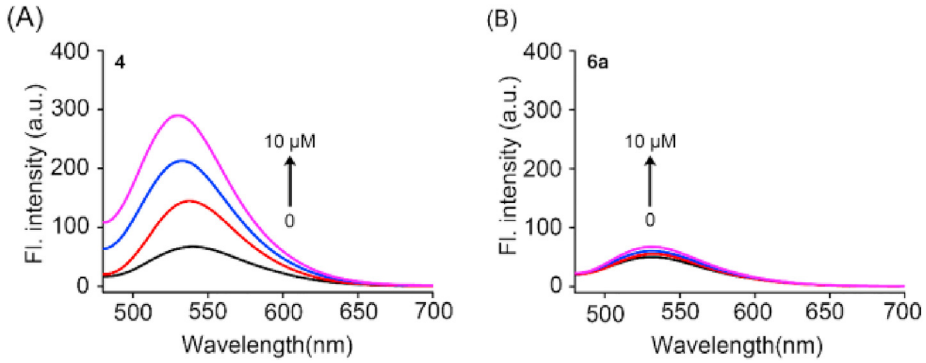

Fig. 3. Fluorescence spectra of 10 μM **4** (A) and 10 μM **6a** (B) upon the addition of various amounts of IDO1 (0, 1, 5, 10 μM) in PBS buffer solution (10 mM, pH = 7.4, containing 1% DMSO). λ_{ex} = 465 nm, slit widths: W_{ex} = 5 nm, W_{em} = 5 nm.

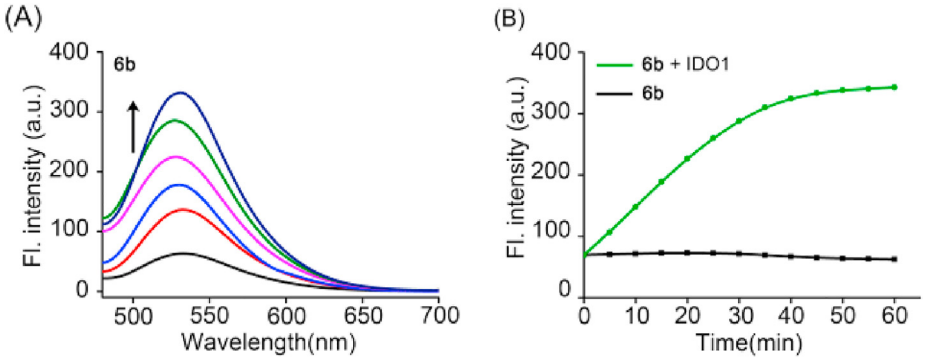

Fig. 4. (A) Fluorescence spectra of **6b** (10 μM) upon the addition of various amounts of IDO1 (0–10 μM, interval 2 μM) in PBS buffer solution. (B) Time course of fluorescence intensity of **6b** (10 μM) in the absence (black) and presence (green) of IDO1 (10 μM) at 532 nm in PBS buffer solution (10 mM, pH = 7.4, containing 1% DMSO). λ_{ex} = 465 nm, slit widths: W_{ex} = 5 nm, W_{em} = 5 nm.

results comprehensively suggested that both **4** and **6b** could sensitively and specifically detect endogenous IDO1 in living cells.

2.6. *In vivo* antitumor efficacy of **6b**

The *in vivo* antitumor efficacy of compound **6b** was further evaluated in CT26 xenograft mouse model which was reported to exhibit high expression of IDO1 [37]. After oral administration for 12 consecutive days at the dose of 100 mg/kg, compound **6b** showed good antitumor activity with the tumor growth inhibition (TGI) rate of 46% (Fig. 7, $P < 0.001$), which was comparable to the positive control epacadostat (TGI = 49%). Furthermore, no significant loss of body weight was observed in mice treated with compound **6b**, indicating low toxicity of this compound.

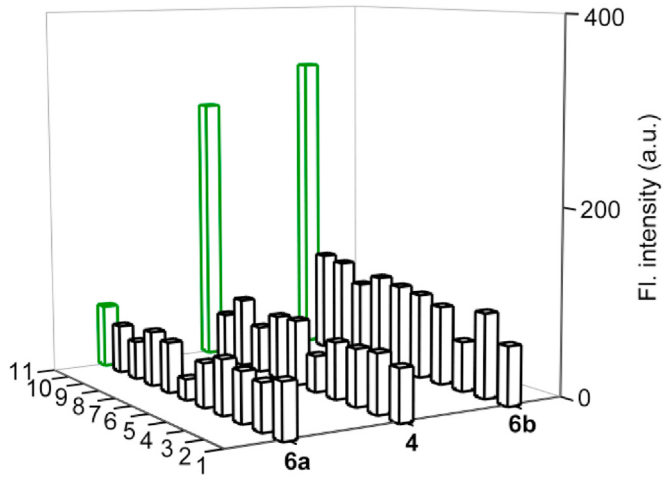

Fig. 5. Selectivity studies. Fluorescence intensity of 10 μM **4** (λ_{em} = 530 nm), 10 μM **6a** (λ_{em} = 531 nm), and 10 μM **6b** (λ_{em} = 532 nm) with the addition of various species in PBS buffer solution. 1, Blank; 2, trypsin; 3, bovine hemoglobin; 4, chymotrypsin; 5, HSA; 6, BSA; 7, lysozyme; 8, *E. coli* β-gal; 9, *A. oryzae* β-gal; 10, GSH; 11, IDO1. λ_{ex} = 465 nm, slit widths: W_{ex} = 5 nm, W_{em} = 5 nm.

3. Conclusions

In conclusion, we rationally designed a series of novel environment-sensitive IDO1 probes, of which probe **6b** displayed excellent fluorescent properties for detection of this enzyme. Further *in vivo* study showed that probe **6b** exhibited good antitumor activity in the CT26 xenograft mouse model, indicating that it is a promising theranostic small-molecule probe. Such probes provide good chemical tools for investigating the biological functions of IDO1. We are looking forward to its application in better understanding the immunotherapy mechanism of IDO1 based on its visibility and diagnosis as well as clinical treatment of patients with IDO1 overexpressed cancer based on its high sensitivity and antitumor efficacy.

4. Experimental section

4.1. Chemistry

The materials used in the experiments were commercially available. Column chromatography was performed on 200–300 mesh silica gel. ^{1}H NMR and ^{13}C NMR spectra were recorded on

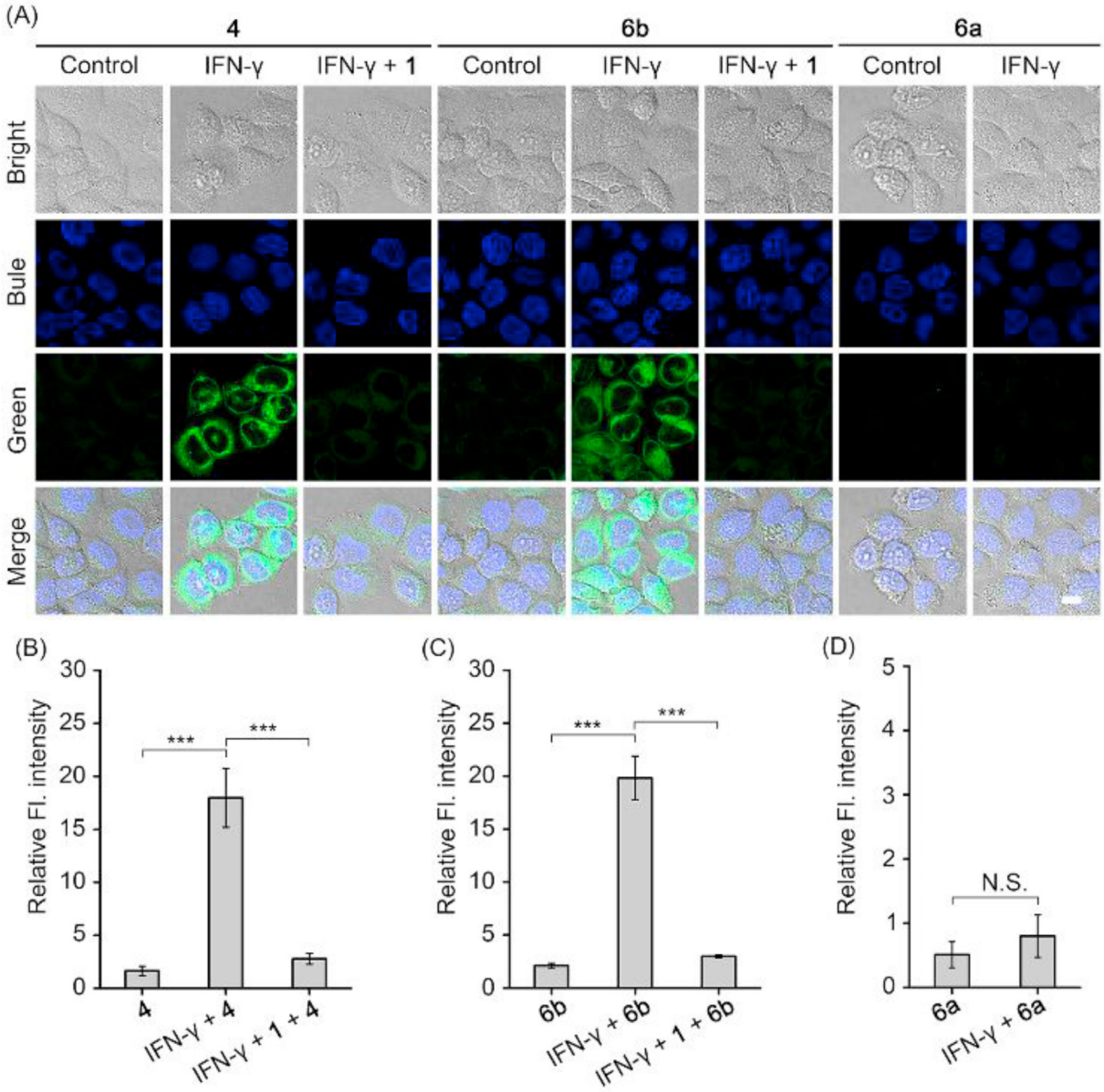

Fig. 6. Imaging of endogenous IDO1 in living Hela cells. (A) Confocal images of living Hela cells stained with **4** (3.5 nM), **6a** (5 nM) and **6b** (5 nM). Column 1, 4 and 7: Hela cells incubated with Hoechst (10 μg/mL, 20 min) and different probes (5 min). Column 2, 5, and 8: Hela cells stimulated with IFN-γ (50 ng/mL, 12 h), followed by incubated with Hoechst (10 μg/mL, 20 min) and different probes (5 min). Column 3 and 6: IFN-γ-stimulated (50 ng/mL, 12 h) Hela cells treated with compound **1** (5 μM, 30 min), followed by incubated with Hoechst (10 μg/mL, 20 min) and different probes (5 min). (B–D) Quantification of the relative fluorescence intensity from column 1–3 (B), column 4–6 (C) and column 7–8 (D). Blue channel: λ_{ex} = 407 nm, λ_{em} = 425–475 nm; green channel: λ_{ex} = 488 nm, λ_{em} = 500–550 nm ***$p < 0.001$, N.S. = not significant, two-sided Student's *t*-test. Scale bar: 10 μm.

Bruker AVANCE300 or AVANCE600 spectrometer (Bruker Company, Germany) with DMSO-d_6 as the solvents and TMS as the internal standard. Chemical shift (δ) was given in ppm and the coupling constant (J) is reported in hertz (Hz). The intermediate **2a** was achieved according to literature [27]. ^{1}H NMR (DMSO-d_6, 600 MHz) δ: 8.12 (dd, J = 2.28, 6.06 Hz, 1 H), 7.74–7.77 (m, 1H), 7.58(t, J = 8.64 Hz, 1H), 6.80–6.82 (m, 1H), 3.50 (d, J = 5.64 Hz, 2H), 3.02 (t, J = 6.00 Hz, 2H).

4.1.1. (Z)-N-(3-Bromo-4-fluorophenyl)-N′-hydroxy-4-((2-((7-nitrobenzo

*4.1.1.1. [c][1,2,5]oxadiazol-4-yl)amino)ethyl)amino)-1,2,5-oxadiazole-3-carboximidamide (**4**).* The intermediate **2a** (1 g, 2.61 mmol), compound **3** (517 mg, 2.61 mmol) and $NaHCO_3$ (263 mg, 3.13 mmol) were dissolved in MeOH (10 mL) and H_2O (5 mL), and the mixture was heated to 60 °C. After stirred for 2 h, the solution was cooled to room temperature, and KOH (292 mg, 5.22 mmol) was added. The mixture was stirred for another 0.5 h, the organic solvent was removed under reduced pressure and the remained mixture was adjusted by 1 M HCl aqueous solution until pH reached 7. The precipitate was filtered, washed with water, and dried to constant weight to obtain the intermediate **4** (380 mg, 28%). Purity >95%. ^{1}H NMR (DMSO-d_6, 600 MHz) δ: 11.38 (s, 1H), 9.48 (s, 1H), 8.88 (s, 1H), 8.51 (d, J = 8.67 Hz, 1 H), 7.13 (t, J = 8.27 Hz, 1 H), 7.07 (dd, J = 2.74, 6.07 Hz, 1 H), 6.74-6.71 (m, 1H), 6.45 (d, J = 9.00 Hz, 2 H), 3.69 (s, 2H), 3.60-3.54 (m, 2H); ^{13}C NMR (DMSO-d_6, 150 MHz) δ: 156.03, 155.79, 152.61, 145.31, 140.53, 139.55, 138.40, 138.37, 125.27, 121.82, 116.53, 116.37, 107.64, 107.35,

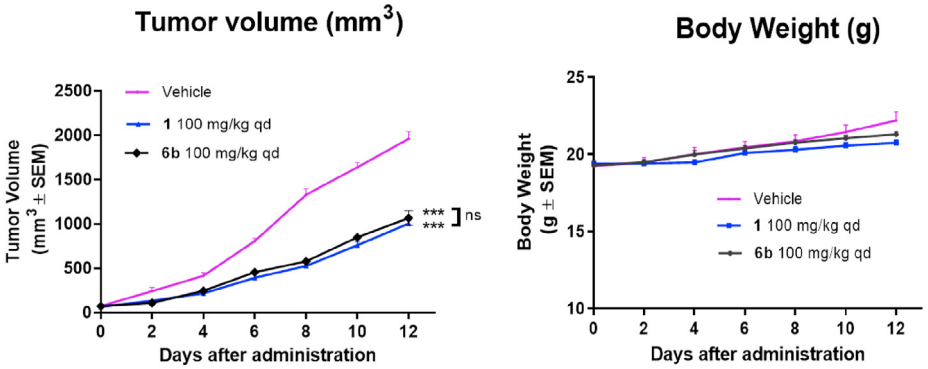

Fig. 7. Antitumor efficacy of compound **1** and compound **6b** in the xenograft model. (A) The efficacy of compound **1** and compound **6b** in the CT26 xenograft model at the dose of 100 mg/kg. (B) The change of body weight for mice that were treated with compound 1 and compound **6b**. Data are presented as the mean ± SEM; n = 5 BalB/C mice per group: (***) $P < 0.001$ versus control group, determined with Student's *t*-test.

99.70, 42.69, 42.38; HRMS (ESI, positive) *m/z* calcd for $C_{17}H_{12}BrFN_9O_5$ $(M - H)^-$ 520.0134, found 522.0152.

4.1.2. (7-Nitrobenzo[c] [1,2,5]oxadiazol-4-yl)glycine (**5a**)

Compound **3** (517 mg, 2.61 mmol), glycine (196 mg, 2.61 mmol) and $NaHCO_3$ (263 mg, 3.13 mmol) were dissolved in MeOH (10 mL) and H_2O (5 mL), and the mixture was heated to 60 °C. The solvent was removed under reduced pressure and the crude product was purified by column chromatography on silica gel (dichloromethane: methanol = 100: 8) to obtain the intermediate **5a** (292 mg, 47%) as an orange solid. ^{1}H NMR (DMSO-d_6, 600 MHz) δ: 12.39 (s, 1 H), 9.44 (s, 1 H), 8.51 (d, J = 8.06 Hz, 1H), 6.44 (d, J = 8.06 Hz, 1H), 3.67 (s, 2H), 2.72 (s, 2H).

4.1.3. 3-((7-Nitrobenzo[c] [1,2,5]oxadiazol-4-yl)amino)propanoic acid (**5b**)

The synthetic procedure of **5b** was similar to that of **5a**. Orange solid, yield 58%. ^{1}H NMR (DMSO-d_6, 600 MHz) δ: 13.09 (s, 1 H), 9.40 (s, 1 H), 8.53 (d, J = 8.90 Hz, 1H), 6.37 (d, J = 8.90 Hz, 1H), 4.28 (s, 2H).

4.1.4. (Z)-N-(2-((4-(N-(3-Bromo-4-fluorophenyl)-N′-hydroxycarbamim-idoyl)-1,2,5-oxa-diazol-3-yl)amino)ethyl)-2-((7-nitrobenzo[c] [1,2,5]oxa-diazol-4-yl)amino)aceta-mide (**6a**)

The intermediate **5a** (238 mg, 1 mmol), compound **2**a (383 mg, 1 mmol), HATU (570 mg, 1.5 mmol) and DIPEA (265 μL, 1.5 mmol) were dissolved in DMF (6 mL) and the mixture was stirred at room temperature for 1 h. Then the solution was poured into saturated NaCl aqueous solution (80 mL) and extracted with ethyl acetate (3 × 15 mL). The organic phase was collected and concentrated under reduced pressure to obtain the crude product, which was subsequently dissolved in MeOH (10 mL) and H_2O (5 mL) along with KOH (78 mg, 2 mmol). The mixture was stirred at room temperature for 0.5 h, and then the solvent was removed under reduced pressure and the crude product was purified by column chromatography on silica gel (dichloromethane: methanol = 100: 1) to obtain the intermediate **6a** (81 mg, 21%) as an orange solid. Purity >95%. ^{1}H NMR (DMSO-d_6, 600 MHz) δ: 9.43 (s, 1 H), 8.50 (t, J = 8.73 Hz, 1H), 8.32 (s, 1H), 8.08 (s, 1H), 7.72 (s, 1H), 7.49–7.66 (m, 1H), 6.55 (s, 1H), 6.24 (s, 1H), 5.56–5.88 (m, 1H), 4.12 (s, 2H), 3.53-3.40 (m, 2H), 3.32 (s, 2H); ^{13}C NMR (DMSO-d_6, 150 MHz) δ:170.59, 156.13, 154.22, 144.82, 140.39, 139.73, 138.44, 138.26, 125.27, 121.93, 116.36, 107.46, 99.68, 44.10, 37.83, 34.20; HRMS (ESI, positive) *m/z* calcd for $C_{19}H_{15}BrFN_{10}O_6$ $(M - H)^-$ 577.0349, found 577.0336.

4.1.5. (Z)-N-(2-((4-(N-(3-Bromo-4-fluorophenyl)-N′-hydroxycarbamim-idoyl)-1,2,5-oxa-diazol-3-yl)amino)ethyl)-2-((7-nitrobenzo[c] [1,2,5]oxa-diazol-4-yl)amino)aceta-mide (**6b**)

The synthetic procedure of **6b** was similar to that of **6b**. Orange solid, yield 14%. Purity >95%. ^{1}H NMR (DMSO-d_6, 600 MHz) δ: 11.45 (s, 1 H), 9.43 (s, 1 H), 8.89 (s, 1H), 8.49 (d, J = 9.80 Hz, 1H), 8.17 (s, 1 H), 7.17 (t, J = 8.17 Hz 1H), 7.06–7.14 (m, 1H), 6.67–6.83 (m, 1H), 6.39 (d, J = 7.80 Hz, 1H), 6.20 (s, 1H), 3.67 (s, 2H), 3.38 (s, 4H), 2.56 (t, J = 5.91 Hz, 2H). ^{13}C NMR (DMSO-d_6, 150 MHz) δ: 170.59, 156.15, 154.95, 153.37, 144.81, 140.37, 139.72, 138.42, 138.24, 125.25, 121.91, 121.35, 116.33, 116.28, 107.54, 107.40, 99.67, 44.09, 37.81, 34.18; HRMS (ESI, positive) *m/z* calcd for $C_{20}H_{19}BrFN_{10}O_6$ $(M + H)^+$ 593.0651, found 593.0657.

4.2. Biological activity

4.2.1. IDO1 enzymatic assay

The assays were performed according to the literature [35]. The reaction mixture contained the test compounds at different concentrations, 20 nM IDO1, 2 mM Trp, 3.5 μM methylene blue, 20 mM ascorbate, and 0.2 mg/mL catalase in 50 mM potassium phosphate buffer (pH 6.5). The absorbance (OD) at 321 nm was read on the WellscanMK-2 microplate reader (Labsystems). The concentration triggering 50% inhibition (IC_{50}) values were calculated using Prism GraphPad software based on nonlinear regression with normalized dose–response fit.

4.2.2. In vitro cytotoxicity assay

Human cervical cancer cell line HeLa or murine colon carcinoma cell line CT26 in the logarithmic phase were harvested and seeded at a density of 6 × 10^3/well in 96-well plates. After incubation for 24 h with 5% CO_2 at 37 °C, the cells were treated with test compounds at different concentrations in three replicates for 72 h. Then they were replaced by100 μL of culture media containing 10% CCK8 kit and the plates were incubated for another 40 min. Then OD values at 480 nm were read on the WellscanMK-2 microplate reader (Labsystems). The concentration triggering 50% inhibition (IC_{50}) values were calculated using Prism GraphPad software based on nonlinear regression with normalized dose–response fit.

4.2.3. Cell based IDO1 assay

Cell based IDO1 assay was carried out according to the literature [17,26]. HeLa cells originating from human cervical cancer in the logarithmic phase were harvested and seeded at a density of 6 × 10^3/well in 96-well plates. After incubation for 24 h with 5% CO_2 at 37 °C, human IFN-γ (50 ng/mL), Trp (15 μg/mL) and test

compounds at different concentrations were added in three replicates. After 48 h, 140 μL of the supernatant was transferred to another 96-well plate, and then 10 μL of 6 N trichloroacetic acid was added, separately. The mixture was incubated for 30 min at 50 °C, and then centrifuged at 2.5×10^3 rpm for 10 min. After that, 100 μL of the supernatant was transferred to another 96-well plate, to which 100 μL of 2% (w/v) p-dimethylaminobenzaldehyde in acetic acid was added. Then OD values at 480 nm were read on the WellscanMK-2 microplate reader (Labsystems). The concentration triggering 50% inhibition (IC_{50}) values were calculated using Prism GraphPad software based on nonlinear regression with normalized dose−response fit.

4.2.4. General fluorescence spectra measurements

A stock solution of probes was prepared in DMSO. All fluorescence titration experiments were performed for 60 min at room temperature using PBS buffer solution. Any changes in the fluorescence intensity were monitored using a fluorescence spectrometer ($\lambda_{ex} = 465$ nm, slit widths: $W_{ex} = 5$ nm, $W_{em} = 5$ nm).

4.2.5. IDO1 cloning, protein expression and purification

The gene of human IDO1 was inserted into an engineered pET21a vector (containing a sumo tag) with BamHI and XhoI as the ligation sites. The resulted construct was transformed into *Escherichia coli* BL21(DE3). The culture was grown in Luria Broth medium to reach an OD600nm of 0.6, and the induction was performed by adding isopropyl–D-galactoside to a final concentration of 0.4 mM. The cells were cultured for another 18 h at 18 °C. Cells were harvested by centrifugation at 6000 rpm for 20 min and then lysed by sonication. After another round of centrifugation at 13,000 rpm for 45 min, the supernatant was collected and was loaded onto a 5-mL HisTrap HP column (GE Healthcare Life Sciences). The IDO1 protein was eluted by a gradient from 0 to 250 mM imidazole within 25 min and buffer exchanged to 50 mM sodium phosphate, pH 8.0 and 500 mM sodium chloride. Ulp1 cleavage of the sumo tag was performed a 13:1 quantity ratio (protein: protease) overnight at 4 °C. The cleaved sample was loaded to the HisTrap HP column again, the flow through was collected and EDTA was added to the sample to the concentration of 2 mM. In the final step, the protein was further purified by gel filtration on a Sperdex75 10/300 GL column (GE Healthcare Life Sciences) in 20 mM Tris, pH = 7.5, 150 mM sodium chloride and 1 mM EDTA.

4.2.6. In vivo studies

CT 26 cells which were in the logarithmic phase were harvested and resuspended in RPMI culture medium. Balb/c female mice (4−5 weeks) were inoculated subcutaneously into the right forelimb with a density of 5×10^5 cells in 0.2 mL. Upon tumor volumes reached approximately 50 mm^3, they were assigned into groups randomly and administered with compounds orally at a dosage of 100 mg/kg every day. The length (a), width (b) of the tumor and body weight of mice were recorded every other day and the tumor volumes were calculated according to $V = 1/2 \times a \times b^2$. When tumor volume of control group approached approximately 2000 mm^3, the mice were sacrificed. Tumor growth inhibition (TGI) was calculated as TGI (%) = ($Vt_{control}$ -$Vt_{compound}$)/$Vt_{control}$ ($Vt_{compound}$ refers to the tumor volume of the test compound group at the last day, while $Vt_{control}$ refers to the to the tumor volume of the control group at the last day).

4.3. Molecular docking simulations

The crystal structure of IDO1 in complex with epacadostat was obtained from protein database bank (PDB code: 5WN8) [33] which was then prepared for docking via the protein preparation tool in Discovery Studio 3.0 [34]. The ligands were also prepared and hydrogens were added to their structures. Then docking experiments were carried out using Gold, in which the parameters were set by default[l] [34][l]. The best conformation was chosen to analyze the ligand-protein interactions between IDO1 and probes, respectively. The figure demonstrating the best conformation was prepared using PyMOL.

Declaration of competing interest

The authors declare that they have no known competing financial interests or personal relationships that could have appeared to influence the work reported in this paper.

Acknowledgements

This work was supported by the National Key R&D Program of China (grant 2017YFA0506000 to C. S.), and National Natural Science Foundation of China (grants 81725020 and 21738002 to C. S., grant 21977082 to Y. G.).

Appendix A. Supplementary data

Supplementary data to this article can be found online at https://doi.org/10.1016/j.ejmech.2021.113163.

References

[1] K.M. Mahoney, P.D. Rennert, G.J. Freeman, Combination cancer immunotherapy and new immunomodulatory targets, Nat. Rev. Drug Discov. 14 (2015) 561−584.
[2] Y. Liu, P. Zheng, Preserving the CTLA-4 checkpoint for safer and more effective cancer immunotherapy, Nat. Immunol. Sci 41 (1) (2020) 4−42.
[3] L.P. Andrews, H. Yano, D.A.A. Vignali, Inhibitory receptors and ligands beyond PD-1, PD-L1 and CTLA-4: breakthroughs or backups, Nat. Immunol. 20 (2019) 1425−1434.
[4] B. Cheng, W.E. Yuan, J. Su, Y. Liu, J. Chen, Recent advances in small molecule based cancer immunotherapy, Eur. J. Med. Chem. 157 (2018) 582−598.
[5] B.R. Huck, L. Kötzner, K. Urbahns, Small molecules drive big improvements in immuno-oncology therapies, Angew. Chem. Int. Ed. 57 (2018) 4412−4428.
[6] D. Dhanak, J.P. Edwards, A. Nguyen, P.J. Tummino, Small-molecule targets in immuno-oncology, Cell Chem. Biol 24 (2017) 1148−1160.
[7] F. Li, R. Zhang, S. Li, J. Liu, Ido1: an important immunotherapy target in cancer treatment, Int. Immunopharm. 47 (2017) 70−77.
[8] B. Ricciuti, G.C. Leonardi, P. Puccetti, F. Fallarino, V. Bianconi, A. Sahebkar, S. Baglivo, R. Chiari, M. Pirro, Targeting indoleamine-2,3-dioxygenase in cancer: scientific rationale and clinical evidence, Pharmacol. Ther. 196 (2019) 105−116.
[9] L. Brochez, I. Chevolet, V. Kruse, The rationale of indoleamine 2,3-dioxygenase inhibition for cancer therapy, Eur. J. Canc. 76 (2017) 167−182.
[10] J.E. Cheong, A. Ekkati, L. Sun, A patent review of Ido1 inhibitors for cancer, Expert Opin. Ther. Pat. 28 (2018) 317−330.
[11] U.F. Röhrig, S.R. Majjigapu, P. Vogel, V. Zoete, O. Michielin, Challenges in the discovery of indoleamine 2,3-dioxygenase 1 (Ido1) inhibitors, J. Med. Chem. 58 (2015) 9421−9437.
[12] G.C. Prendergast, W.P. Malachowski, J.B. DuHadaway, A.J. Muller, Discovery of Ido1 inhibitors: from bench to bedside, Canc. Res. 77 (2017) 6795−6811.
[13] B.W. Labadie, R. Bao, J.J. Luke, Reimagining Ido pathway inhibition in cancer immunotherapy via downstream focus on the tryptophan-kynurenine-aryl hydrocarbon Axis, Clin. Canc. Res. 25 (2019) 1462−1471.
[14] G.V. Long, R. Dummer, O. Hamid, T.F. Gajewski, C. Caglevic, S. Dalle, A. Arance, M.S. Carlino, J.J. Grob, T.M. Kim, L. Demidov, C. Robert, J. Larkin, J.R. Anderson, J. Maleski, M. Jones, S.J. Diede, T.C. Mitchell, Epacadostat plus pembrolizumab versus placebo plus pembrolizumab in patients with unresectable or metastatic melanoma (ECHO-301/KEYNOTE-252): a phase 3, randomised, double-blind study, Lancet Oncol. 20 (2019) 1083−1097.
[15] S. Cai, X. Yang, P. Chen, X. Liu, J. Zhou, H. Zhang, Design, synthesis and biological evaluation of bicyclic carboxylic acid derivatives as Ido1 inhibitors, Bioorg. Chem. (2019) 103356.
[16] H. Zhang, K. Liu, Q. Pu, A. Achab, M.J. Ardolino, M. Cheng, Y. Deng, A.C. Doty, H. Ferguson, X. Fradera, I. Knemeyer, R. Kurukulasuriya, Y.H. Lam, C.A. Lesburg, T.A. Martinot, M.A. McGowan, J.R. Miller, K. Otte, P.J. Biju, N. Sciammetta, N. Solban, W. Yu, H. Zhou, X. Wang, D.J. Bennett, Y. Han, Discovery of amino-cyclobutarene-derived indoleamine-2,3-dioxygenase 1 (Ido1) inhibitors for cancer immunotherapy, ACS Med. Chem. Lett. 10 (2019) 1530−1536.

[17] Y. Zou, Y. Hu, S. Ge, Y. Zheng, Y. Li, W. Liu, W. Guo, Y. Zhang, Q. Xu, Y. Lai, Effective virtual screening strategy toward heme-containing proteins: identification of novel Ido1 inhibitors, Eur. J. Med. Chem. 184 (2019) 111750.
[18] Q. Du, X. Feng, Y. Wang, X. Xu, Y. Zhang, X. Qu, Z. Li, J. Bian, Discovery of phosphonamidate Ido1 inhibitors for the treatment of non-small cell lung cancer, Eur. J. Med. Chem. 182 (2019) 111629.
[19] Y. Zhou, J. Peng, P. Li, H. Du, Y. Li, L. Zhang, W. Sun, X. Liu, Z. Zuo, Discovery of novel indoleamine 2,3-dioxygenase 1 (Ido1) inhibitors by virtual screening, Comput. Biol. Chem. 78 (2019) 306–316.
[20] U.F. Rohrig, A. Reynaud, S.R. Majjigapu, P. Vogel, F. Pojer, V. Zoete, Inhibition mechanisms of indoleamine 2,3-dioxygenase 1 (Ido1), J. Med. Chem. 62 (2019) 8784–8795.
[21] K.N. Pham, A. Lewis-Ballester, S.R. Yeh, Structural basis of inhibitor selectivity in human indoleamine 2,3-dioxygenase 1 and tryptophan dioxygenase, J. Am. Chem. Soc. 141 (2019) 18771–18779.
[22] M.T. Nelp, P.A. Kates, J.T. Hunt, J.A. Newitt, A. Balog, D. Maley, X. Zhu, L. Abell, A. Allentoff, R. Borzilleri, H.A. Lewis, Z. Lin, S.P. Seitz, C. Yan, J.T. Groves, Immune-modulating enzyme indoleamine 2,3-dioxygenase is effectively inhibited by targeting its apo-form, Proc. Natl. Acad. Sci. U. S. A 115 (2018) 3249–3254.
[23] D. Yang, S. Zhang, X. Fang, L. Guo, N. Hu, Z. Guo, X. Li, S. Yang, J.C. He, C. Kuang, Q. Yang, N-Benzyl/Aryl substituted tryptanthrin as dual inhibitors of indoleamine 2,3-dioxygenase and tryptophan 2,3-dioxygenase, J. Med. Chem. 62 (2019) 9161–9174.
[24] K. Fang, G. Dong, Y. Li, S. He, Y. Wu, S. Wu, W. Wang, C. Sheng, Discovery of novel indoleamine 2,3-dioxygenase 1 (Ido1) and histone deacetylase (HDAC) dual inhibitors, ACS Med. Chem. Lett. 9 (2018) 312–317.
[25] K. Fang, G. Dong, H. Wang, S. He, S. Wu, W. Wang, C. Sheng, Improving the potency of cancer immunotherapy by dual targeting of Ido1 and DNA, ChemMedChem 13 (2018) 30–36.
[26] K. Fang, S. Wu, G. Dong, Y. Wu, S. Chen, J. Liu, W. Wang, C. Sheng, Discovery of Ido1 and DNA dual targeting antitumor agents, Org. Biomol. Chem. 15 (2017) 9992–9995.
[27] E.W. Yue, R. Sparks, P. Polam, D. Modi, B. Douty, B. Wayland, B. Glass, A. Takvorian, J. Glenn, W. Zhu, M. Bower, X. Liu, L. Leffet, Q. Wang, K.J. Bowman, M.J. Hansbury, M. Wei, Y. Li, R. Wynn, T.C. Burn, H.K. Koblish, J.S. Fridman, T. Emm, P.A. Scherle, B. Metcalf, A.P. Combs, INCB24360 (epacadostat), a highly potent and selective indoleamine-2,3-dioxygenase 1 (Ido1) inhibitor for immuno-oncology, ACS Med. Chem. Lett. 8 (2017) 486–491.
[28] Y.D. Zhuang, P.Y. Chiang, C.W. Wang, K.T. Tan, Environment-sensitive fluorescent turn-on probes targeting hydrophobic ligand-binding domains for selective protein detection, Angew. Chem. Int. Ed. 52 (2013) 8124–8128.
[29] R.P. Huijbregts, A.I. de Kroon, B. de Kruijff, Rapid transmembrane movement of C6-NBD-labeled phospholipids across the inner membrane of Escherichia coli, Biochim. Biophys. Acta 1280 (1996) 41–50.
[30] K. Cui, Z. Chen, Z. Wang, G. Zhang, D. Zhang, A naked-eye visible and fluorescence "turn-on" probe for acetyl-cholinesterase assay and thiols as well as imaging of living cells, Analyst 136 (2011) 191–195.
[31] W. Jiang, Q. Fu, H. Fan, J. Ho, W. Wang, A highly selective fluorescent probe for thiophenols, Angew. Chem. Int. Ed. 46 (2007) 8445–8448.
[32] L. Yi, Z. Xi, Thiolysis of NBD-based dyes for colorimetric and fluorescence detection of H(2)S and biothiols: design and biological applications, Org. Biomol. Chem. 15 (2017) 3828–3839.
[33] A. Lewis-Ballester, K.N. Pham, D. Batabyal, S. Karkashon, J.B. Bonanno, T.L. Poulos, S.R. Yeh, Structural insights into substrate and inhibitor binding sites in human indoleamine 2,3-dioxygenase 1, Nat. Commun. 8 (2017) 1693.
[34] G. Jones, P. Willett, R.C. Glen, A.R. Leach, R. Taylor, Development and validation of a genetic algorithm for flexible docking, J. Mol. Biol. 267 (1997) 727–748.
[35] M.F. Cheng, M.S. Hung, J.S. Song, S.Y. Lin, F.Y. Liao, M.H. Wu, W. Hsiao, C.L. Hsieh, J.S. Wu, Y.S. Chao, C. Shih, S.Y. Wu, S.H. Ueng, Discovery and structure-activity relationships of phenyl benzenesulfonylhydrazides as novel indoleamine 2,3-dioxygenase inhibitors, Bioorg. Med. Chem. Lett 24 (2014) 3403–3406.
[36] J.E. Cheong, L. Sun, Targeting the Ido1/TDO2-KYN-AhR pathway for cancer immunotherapy - challenges and opportunities, Trends Pharmacol. Sci. 39 (2018) 307–325.
[37] H.K. Koblish, M.J. Hansbury, K.J. Bowman, G. Yang, C.L. Neilan, P.J. Haley, T.C. Burn, P. Waeltz, R.B. Sparks, E.W. Yue, A.P. Combs, P.A. Scherle, K. Vaddi, J.S. Fridman, Hydroxyamidine inhibitors of indoleamine-2,3-dioxygenase potently suppress systemic tryptophan catabolism and the growth of Ido-expressing tumors, Mol. Canc. Therapeut. 9 (2010) 489–498.